Progress In Electromagnetics Research B, Vol. 9, 165–178, 2008

A NUMERICAL FILTER TO REMOVE THE FIELD SCATTERED BY THE EDGES OF A FINITE GROUND PLANE FROM MEASURED DATA

E. Di Giampaolo

Dipartimento di Informatica, Sistemi e Produzione
Università di Roma Tor Vergata
Via del Politecnico 1, Roma 00133, Italy

Abstract—The measurement of the field radiated from an antenna placed above a finite ground plane experiences the effects of the field scattered by the edges of the ground plane. A new numerical method to remove these effects from measured data is presented here. It resorts to the image theorem and can be used for both near-field and far-field measurements. A simple and effective algorithm has been developed to apply that method to fields described by means of spherical wave expansion. A numerical validation shows the effectiveness of the method.

1. INTRODUCTION

The experimental characterisation of antennas mounted on a ground plane is applied to a large class of antennas, e.g., antennas for aerospace and automotive applications, mounted on or integrated in vehicle surfaces [1, 2]. The modelling of antennas is performed by means of numerical methods [3–5] that may permit to take into account the surface where the antenna will be mounted, but usually an infinite ground plane is used in place of the real surface. Preliminary measurements with the antenna mounted on a flat ground plane are frequently performed during the modelling stage in order to reveal the adequacy of the model, but the measured data experiences the effects of the field scattered by the edges of the finite size ground plane. This makes it difficult to compare a theoretical field prediction with that measured experimentally. In particular, the scattered field interferes with the field radiated by the antenna producing a radiation pattern with back-side lobes and front-side ripple. The effects of the finite ground plane (FGP) on the radiation pattern of antennas have

been studied by several researchers in order to improve the radiation characteristics of the antennas [6–12] as well as to eliminate the field scattered by the edges of the ground plane from measured data [13–17]. In this case, time gating [16, 17] is used to remove the scattered fields from measured data while absorbent materials placed along the edges [14, 15] are used to reduce the effects of the unwanted scattered field. These techniques, however, have some drawbacks: in particular they do not permit to determine the radiation pattern at the angles near the horizon with sufficient accuracy. An alternative is given by the numerical technique proposed by Williams [13] based on the subtraction of the scattered field measured on the backside of the FGP (i.e. the side not hosting the antenna) from that measured on the front side. The theoretical foundation of this technique is based on the Geometrical Theory of Diffraction [18], and it exploits the symmetry of the field diffracted by the edges of an infinitesimally thin FGP with respect to the plane where the FGP lies. This technique has been successfully applied to far-field measured data and has been limited to flush-mounted antennas on thin ground planes.

Currently near-field measurement systems are widely used. They are suitable for many kinds of antennas and are an attractive alternative to the conventional far-field measurement if the far-field distance is large. The field is gathered in the near-field, and a near-field to far-field transformation is performed to determine the far-field [19–25]. Near-field multi-probe systems [26–29] collect the field radiated from the antenna under test on a spherical surface which includes both the antenna and the FGP. A numerical processing of measured data makes it possible to describe the field by means of a spherical waves expansion (SWE) [30]. To recover the spherical wave spectrum of the antenna as if it was placed on an infinite ground plane, the field scattered by the FGP edges has to be removed from the SWE. In this paper we demonstrate that the technique proposed in [13] can also be used in near-field measurement and is not limited to flush-mounted antennas. This technique is a consequence of the image theorem which does not depend on the source position or on the far-field approximation. Moreover, a simple and effective algorithm is given to remove the components of the field scattered by the FGP edges from the SWE of the measured near/far-field. It exploits the symmetry of Maxwell's equations together with the symmetry of the associated Legendre functions. The paper is organised into three Sections: Section 1 shows the theoretical description of the method demonstrating its applicability to both near-field and not flush-mounted antennas; Section 2 describes the algorithm for SWE, while Section 3 is devoted to the validation of the method by means of a numerical analysis.

2. THEORETICAL OVERVIEW

A measurement system consisting of an FGP and a radiating source S is placed in an unbounded medium (e.g., free space) with constitutive parameters ε and μ (permittivity and permeability, respectively). The FGP, supposed to be an infinitesimally thin perfect electric conductor, lies on the plane $z = 0$ of a Cartesian reference system (x, y, z) with unit vectors $(\underline{\hat{x}}, \underline{\hat{y}}, \underline{\hat{z}})$ (Fig. 1). The source S, represented by means of the vector current densities $\underline{J}$ and $\underline{M}$ (electric and magnetic, respectively), is supposed to be at a given distance from the FGP in the half space $z > 0$. The electromagnetic field vectors $(\underline{E}, \underline{H})$ are solutions to Maxwell's equations with sources $\underline{J}$ and $\underline{M}$, and perfect electric conductor boundary conditions on the FGP. The electric current density $\underline{J}_s = \underline{\hat{z}} \times \underline{H}$ induced on the surface of the FGP is parallel to the plane $z = 0$.

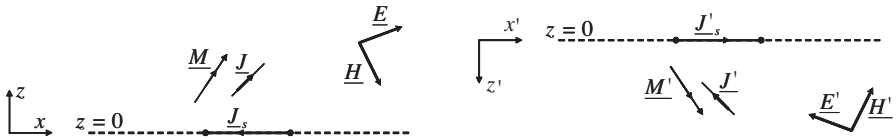

Figure 1. A two dimensional schema of the image theorem applied to an antenna above an FGP. (a) Assigned arrangement, (b) Image arrangement.

The image field (E', H') of (E, H) image of $(\underline{E},\underline{H})$ with respect to the plane $z = 0$ is obtained with the following transformation

$$\underline{\hat{z}} \times \underline{E'} = -\underline{\hat{z}} \times \underline{E} \tag{1a}$$

$$\underline{\hat{z}} \times \underline{H'} = \underline{\hat{z}} \times \underline{H} \tag{1b}$$

$$\underline{\hat{z}} \cdot \underline{E'} = \underline{\hat{z}} \cdot \underline{E} \tag{1c}$$

$$\underline{\hat{z}} \cdot \underline{H'} = -\underline{\hat{z}} \cdot \underline{H}. \tag{1d}$$

It is a solution to Maxwell's equations in the whole space with coordinate reference system (x', y', z') where $x' = x$, $y' = y$ and $z' = -z$. The image sources are $\underline{J'}$ with $\underline{\hat{z}} \times \underline{J'} = -\underline{\hat{z}} \times \underline{J}$, $\underline{\hat{z}} \cdot \underline{J'} = \underline{\hat{z}} \cdot \underline{J}$ and $\underline{M'}$ with $\underline{\hat{z}} \times \underline{M'} = \underline{\hat{z}} \times \underline{M}$, $\underline{\hat{z}} \cdot \underline{M'} = -\underline{\hat{z}} \cdot \underline{M}$ while $\underline{J'}_s = -\underline{J}_s$ is the image of the induced current.

By superimposing $(\underline{E}, \underline{H})$ and $(\underline{E'}, \underline{H'})$ we obtain a new field $\underline{E}_1 = \underline{E} + \underline{E'}$ and $\underline{H}_1 = \underline{H} + \underline{H'}$ which is a solution to Maxwell's equations in the whole space with sources $(\underline{J}, \underline{M})$ and $(\underline{J'}, \underline{M'})$. $(\underline{E}_1, \underline{H}_1)$ has particular symmetries with respect to the plane $z = 0$ and satisfies the

electric wall boundary condition on the plane $z = 0$ as $\underline{\hat{z}} \times \underline{E}_1(x, y, 0) = 0$ and $\underline{\hat{z}} \cdot \underline{H}_1(x, y, 0) = 0$. Therefore, in the half space $z > 0$, ($\underline{E}_1$, $\underline{H}_1$) can be considered a solution to Maxwell's equations with source $\underline{J}$ and $\underline{M}$ in front of an infinite perfect electric conductor plane placed at $z = 0$. This demonstrates that the image theorem permits the fields scattered by the edges of an infinitesimally thin finite ground plane to be removed independently from the position and the kind of radiating source. If $\underline{E}$ is a measured electric field, the image $\underline{E'}$ is obtained overturning the measured data with respect to $z = 0$, so that

$$\underline{E}_{1x}(x, y, z) = \underline{E}_x(x, y, z) - \underline{E}_x(x, y, -z) \tag{2a}$$

$$\underline{E}_{1y}(x, y, z) = \underline{E}_y(x, y, z) - \underline{E}_y(x, y, -z) \tag{2b}$$

$$\underline{E}_{1z}(x, y, z) = \underline{E}_z(x, y, z) + \underline{E}_z(x, y, -z) \tag{2c}$$

Subtraction technique [13], demonstrated for the hard component of the edge diffracted field, corresponds to Equation (2c).

Using a ground plane with a finite thickness we also have to consider the induced electric currents on the perimeter sides (i.e., the sides concerning the thickness). These currents have a component parallel to the normal vector of the ground plane that does not vanish by using the image theorem. Therefore it is not possible to eliminate their contribution to the final field. The effect of the perimeter currents depends on the thickness and the size of the ground plane. In the case of a small ground plane the antenna couples strongly with the perimeter sides making the perimeter current stronger than that of a large ground plane. In practical applications, however, the contribution produced by perimeter currents can be made small using a ground plane sufficiently thin and large with respect to the wavelength.

3. APPLICATION TO SPHERICAL NEAR-FIELD DATA

In a spherical near-field measurement system all electromagnetic field sources are inside a spherical surface of radius r_0, while the field is measured at points of a sphere of radius $r > r_0$ contained in a source-free space. The field is generally expressed with respect to a spherical coordinate system (r, θ, ϕ) with unit vectors $(\underline{\hat{r}}, \underline{\hat{\theta}}, \underline{\hat{\phi}})$. If the origin of the spherical system is placed on the plane including the FGP (i.e., $z = 0$) the image of the field can be obtained overturning measured data with respect to $\theta = \pi/2$, θ being the polar angle from the positive z-axis, while r is the radial distance from the reference origin and ϕ the azimuth angle from the positive x-axis. The superimposed electric

field has components $(E_{1r}, E_{1\theta}, E_{1\phi})$ with

$$E_{1\theta}(r,\theta,\phi) = E_\theta(r,\theta,\phi) + E_\theta(r,\pi-\theta,\phi) \tag{3a}$$
$$E_{1\phi}(r,\theta,\phi) = E_\phi(r,\theta,\phi) - E_\phi(r,\pi-\theta,\phi) \tag{3b}$$
$$E_{1r}(r,\theta,\phi) = E_r(r,\theta,\phi) - E_r(r,\pi-\theta,\phi) \tag{3c}$$

(E_r, E_θ, E_ϕ) being the components of the measured electric field.

The measured field can be described by means of an SWE whose coefficients are determined from the knowledge of the tangential components of either $\underline{E}$ or $\underline{H}$ on the measurement sphere. The SWE of an electric (magnetic) field is the weighted sum of a number of transverse electric and transverse magnetic spherical wave functions defined in the spherical coordinates system. The sum coefficients are retrieved from measured data and their number depends on the radius r_0 and on the accuracy required. The components of the electric field in terms of spherical wave functions are [30]

$$E_r(r,\theta,\phi) = \sum_{n=1}^{N}\sum_{m=-n}^{n} A_{mn} e^{jm\phi}\left\{\frac{n(n+1)}{kr} R_{mn}(\theta) a^2_{mn} h^{(2)}_n(kr)\right\} \tag{4a}$$

$$E_\theta(r,\theta,\phi) = \sum_{n=1}^{N}\sum_{m=-n}^{n} A_{mn} e^{jm\phi}\left\{jG_{\theta\,mn}(\theta) a^1_{mn} h^{(2)}_n(kr) + F_{\theta\,mn}(\theta)\, a^2_{mn} \frac{1}{kr}\frac{d}{d(kr)}\left[kr\, h^{(2)}_n(kr)\right]\right\} \tag{4b}$$

$$E_\phi(r,\theta,\phi) = \sum_{n=1}^{N}\sum_{m=-n}^{n} A_{mn} e^{jm\phi}\left\{jG_{\phi\,mn}(\theta) a^2_{mn} \frac{1}{kr}\frac{d}{d(kr)}\left[kr h^{(2)}_n(kr)\right] - F_{\phi\,mn}(\theta) a^1_{mn} h^{(2)}_n(kr)\right\} \tag{4c}$$

where $\{a^1_{mn}, a^2_{mn}\}$ are the coefficients, $A_{mn} = \frac{k}{\sqrt{\eta}}\frac{1}{\sqrt{2\pi}}\frac{1}{\sqrt{n(n+1)}}(-\frac{m}{|m|})^m$ is a normalization factor, $k = \omega\sqrt{\mu\varepsilon}$ is the propagation constant, $\eta = \sqrt{\frac{\varepsilon}{\mu}}$ the specific admittance of the medium, while ω is the angular frequency. Spherical wave functions are products of elementary functions that are separated with respect to their dependence on radial, polar and azimuthal coordinates. The radial dependence is expressed through the spherical Hankel function of the second kind $h^{(2)}_n(kr)$ and nth order, while the exponential function $e^{jm\phi}$ expresses the azimuthal dependence. The polar dependence, instead, is expressed through three

functions, all defined in the interval $0 \leq \theta \leq \pi$

$$R_{r\,mn}(\theta) = \overline{P}_n^{|m|}(\cos\theta) \tag{5a}$$

$$F_{\theta\,mn}(\theta) = F_{\phi\,mn}(\theta) = \frac{d}{d\theta}\overline{P}_n^{|m|}(\cos\theta) \tag{5b}$$

$$G_{\theta\,mn}(\theta) = G_{\phi\,mn}(\theta) = \frac{m}{\sin\theta}\overline{P}_n^{|m|}(\cos\theta) \tag{5c}$$

where $\overline{P}_n^{|m|}(\cos\theta)$ is the normalized associated Legendre function of the mth order and nth degree. As only the associated Legendre functions depend on the polar coordinate θ, we use overturned functions ($R_{r\,mn}(\pi-\theta)$, $F_{\theta(\phi)\,mn}(\pi-\theta)$, $G_{\theta(\phi)\,mn}(\pi-\theta)$) to describe the image field $\underline{E'}$. The superimposed field $\underline{E}_1$ is obtained from Equations (4) inserting the following functions

$$R_{1r\,mn}(\theta) = R_{r\,mn}(\theta) - R_{r\,mn}(\pi-\theta) \tag{6a}$$

$$F_{1\theta\,mn}(\theta) = F_{\theta\,mn}(\theta) + F_{\theta\,mn}(\pi-\theta) \tag{6b}$$

$$F_{1\phi\,mn}(\theta) = F_{\phi\,mn}(\theta) - F_{\phi\,mn}(\pi-\theta) \tag{6c}$$

$$G_{1\theta\,mn}(\theta) = G_{\theta\,mn}(\theta) + G_{\theta\,mn}(\pi-\theta) \tag{6d}$$

$$G_{1\phi\,mn}(\theta) = G_{\phi\,mn}(\theta) - G_{\phi\,mn}(\pi-\theta) \tag{6e}$$

in place of $R_{r\,mn}(\theta)$, $F_{\theta(\phi)\,mn}(\theta)$ and $G_{\theta(\phi)\,mn}(\theta)$, respectively.

But the associated Legendre functions $\overline{P}_n^{|m|}(\cos\theta)$ have particular properties of symmetry with respect to $\theta = \pi/2$. Odd order and odd degree functions are even (with respect to $\theta = \pi/2$), while odd order and even degree functions are odd. Even order and even degree functions are even, while even order and odd degree functions are odd. Consequently, the overturned functions $\overline{P}_n^{|m|}(\cos(\pi-\theta))$, $\frac{m}{\sin(\pi-\theta)}\overline{P}_n^{|m|}(\cos(\pi-\theta))$ and $\frac{d}{d\theta}\overline{P}_n^{|m|}(\cos(\pi-\theta))$ are either additive or additive inverse of $\overline{P}_n^{|m|}(\cos\theta)$, $\frac{m}{\sin(\theta)}\overline{P}_n^{|m|}(\cos(\theta))$ and $\frac{d}{d\theta}\overline{P}_n^{|m|}(\cos(\theta))$, respectively, in accordance with their order and their degree. Exploiting these properties we have:

$$\left.\begin{aligned} &R_{1r\,mn}(\theta) = 2R_{r\,mn}(\theta) \\ &F_{1\theta\,mn}(\theta) = 2F_{\theta\,mn}(\theta) \\ &G_{1\phi\,mn}(\theta) = 2G_{\phi\,mn}(\theta) \\ &F_{1\phi\,mn}(\theta) = 0 \\ &G_{1\theta\,mn}(\theta) = 0 \end{aligned}\right\} \quad \text{if } |m|+n \text{ is odd} \tag{7a}$$

$$\left.\begin{array}{l} R_{1r\,mn}(\theta) = 0 \\ F_{1\theta\,mn}(\theta) = 0 \\ G_{1\phi\,mn}(\theta) = 0 \\ F_{1\phi\,mn}(\theta) = 2F_{\phi\,mn}(\theta) \\ G_{1\theta\,mn}(\theta) = 2G_{\theta\,mn}(\theta) \end{array}\right\} \quad \text{if } |m|+n \text{ is even} \tag{7b}$$

As a consequence of these properties, coefficients $\{a^1_{mn}, a^2_{mn}\}$ associated to vanishing functions of (7) can be removed, while the others can be doubled. Thus, a set of new coefficients $\{c^1_{mn}, c^2_{mn}\}$ can be obtained from the set $\{a^1_{mn}, a^2_{mn}\}$ by means of the following relationships:

$$c^1_{m,n} = \begin{cases} 2a^1_{m,n} & \text{if } |m|+n \text{ is even} \\ 0 & \text{if } |m|+n \text{ is odd} \end{cases} \tag{8a}$$

$$c^2_{m,n} = \begin{cases} 0 & \text{if } |m|+n \text{ is even} \\ 2a^2_{m,n} & \text{if } |m|+n \text{ is odd.} \end{cases} \tag{8b}$$

The field $\underline{E}_1$ calculated inserting $\{c^1_{mn}, c^2_{mn}\}$ directly into the SWE (4) in place of $\{a^1_{mn}, a^2_{mn}\}$ is the superimposition of the measured field $\underline{E}$ and its image $\underline{E}'$. Moreover, $\underline{E}_1$ satisfies the perfect electric conductor boundary condition on the whole plane $z = 0$ owing to the following property

$$\left.\begin{array}{l} R_{r\,mn}(\theta = \pi/2) = 0 \\ G_{\phi\,mn}(\theta = \pi/2) = 0 \end{array}\right\} \text{if } |m|+n \text{ is odd} \qquad F_{\phi\,mn}(\theta = \pi/2) = 0 \quad \text{if } |m|+n \text{ is even} \tag{9}$$

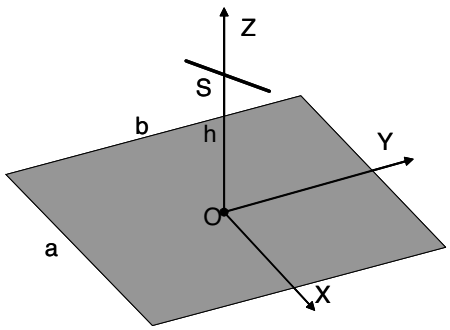

Figure 2. Arrangement of a dipole above an FGP. Dipole S is parallel to the FGP but skewed with respect to its sides. $a = b = 2\lambda$ length of the sides of the FGP, $h = \lambda$ distance between the dipole and the FGP (λ is the wavelength).

Therefore, restricting the domain of Equations (4) to the interval $0 \leq \theta \leq \frac{\pi}{2}$ and using the coefficients $\{c^1_{mn}, c^2_{mn}\}$ we have the SWE of the field radiated by a given antenna placed above an infinite ground plane. The power flow associated to that field is half of

$$P = \frac{1}{2} \sum_{n=1}^{N} \sum_{m=-n}^{n} \left[\left| c^1_{mn} \right|^2 + \left| c^2_{mn} \right|^2 \right] \tag{10}$$

which is the real part of the flux of the complex Poynting vector computed on the whole solid angle.

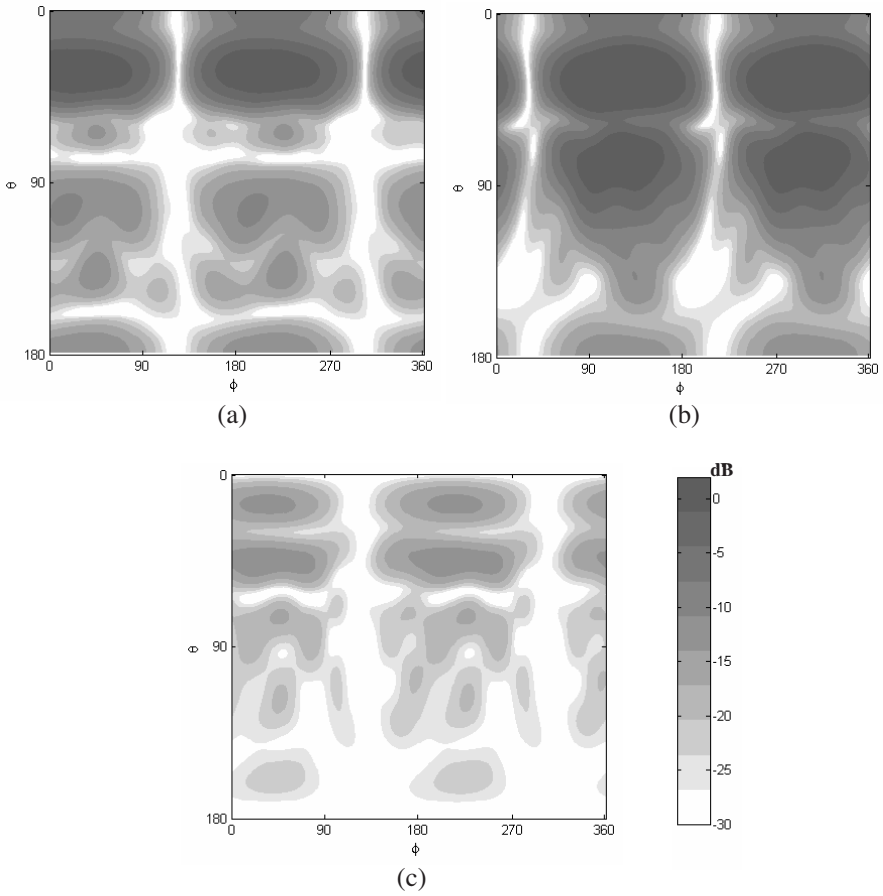

Figure 3. Map on the $(\theta - \phi)$ plane of the magnitude of the near-field of the arrangement of Fig. 2. (a) Polar component, (b) Azimuthal component, (c) Radial component. Colour scale in dB. Field obtained by method of moments.

4. NUMERICAL ANALYSIS AND DISCUSSION

The method has been validated using synthetic data produced by means of a numerical analysis based on the method of moments [31]. The validation procedure is based on the comparison, component by component, between the field obtained with the proposed method ($\underline{E}^I$) and that obtained resorting to an infinite ground plane ($\underline{E}^{IGP}$). Both near-field and far-field of different arrangements of antennas and of FGP were calculated on a sphere whose centre lay on the plane of the FGP. To determine the discrepancy between $\underline{E}^I$ and $\underline{E}^{IGP}$ the

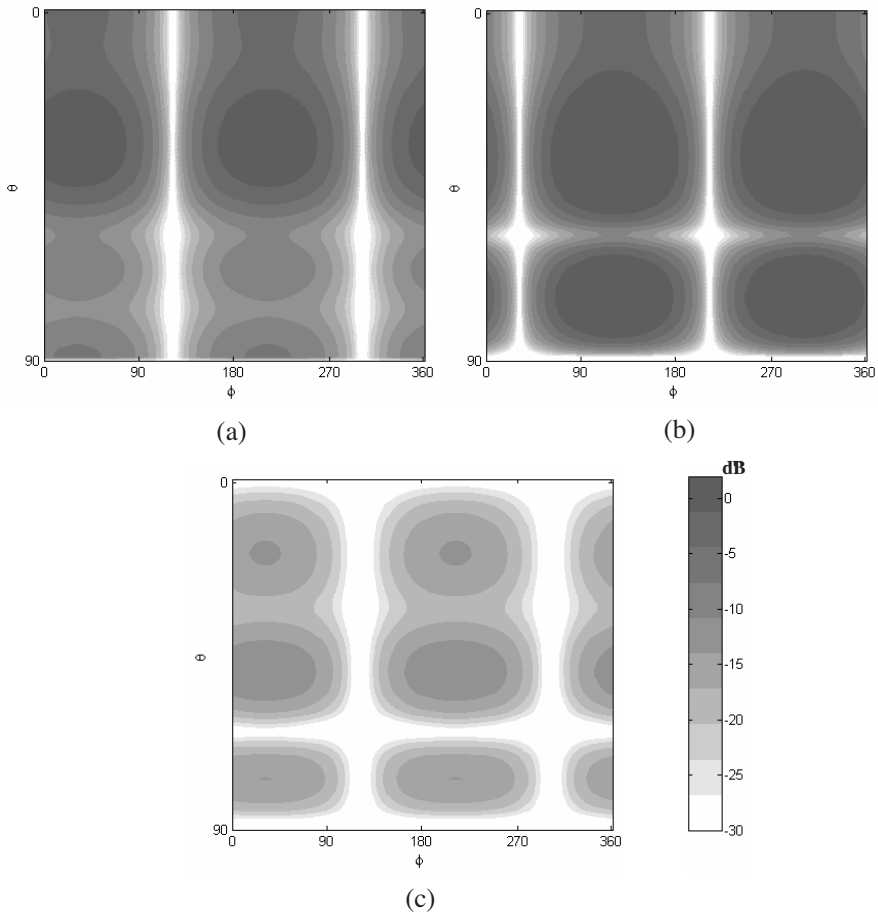

Figure 4. Map on the $(\theta - \phi)$ plane of the magnitude of the near-field obtained with the proposed method. (a) Polar component, (b) Azimuthal component, (c) Radial component. Colour scale in dB.

relative error $e_{\Diamond}(r,\theta,\phi) = \frac{||E^{I}_{\Diamond}(r,\theta,\phi)|-|E^{IGP}_{\Diamond}(r,\theta,\phi)||}{|E^{IGP}_{\Diamond}(r,\theta,\phi)|}$, where the symbol '$\Diamond$' indicates a specific field component in the spherical coordinates system, was calculated. $e_{\Diamond}$ concerns the numerical noise, it has its maximum values at points where the field is weak, but it does not exceed one per cent in all components of the field and in all arrangements considered. For this reason only an arrangement concerning a near-field calculation has been reported here.

A squared FGP with sides two wavelengths long is centered at

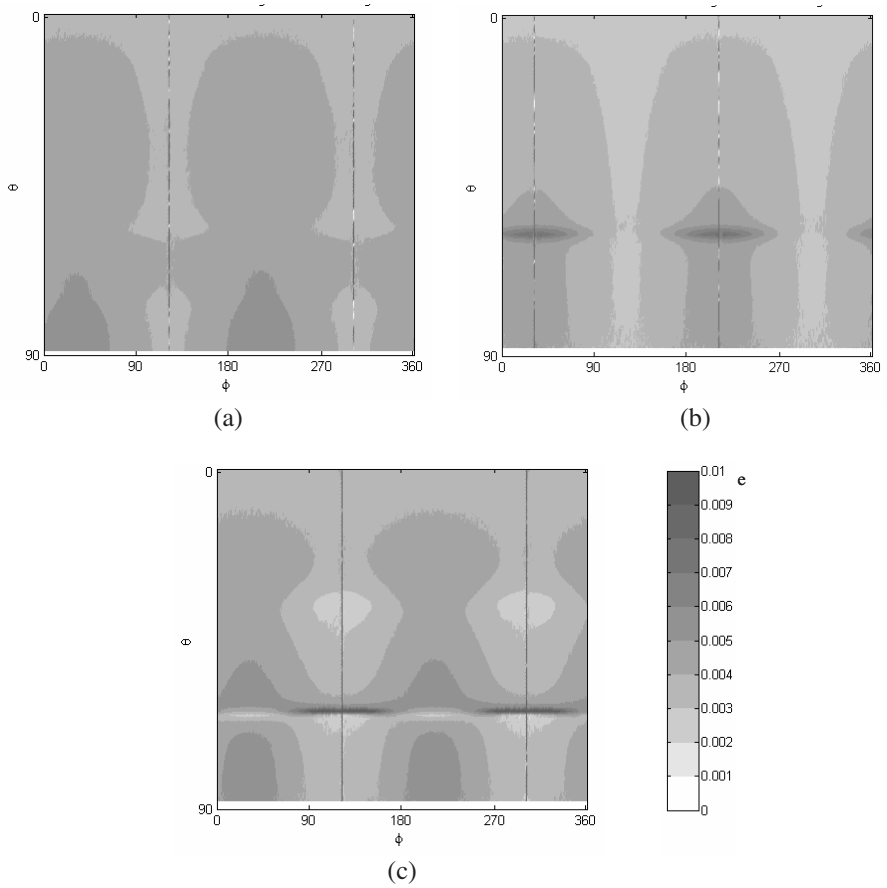

Figure 5. Map on the $(\theta - \phi)$ plane of the relative error between the magnitude of the near-field obtained with the proposed method and that calculated using an infinite ground plane. (a) Polar component, (b) Azimuthal component, (c) Radial component. Colour scale is linear.

the origin of a Cartesian reference system. A half wavelength dipole, parallel to the FGP and with a voltage source at the gap, is placed at a wavelength far from the FGP (Fig. 2). The spherical surface where the field is determined has its centre at the origin of the reference system and radius three wavelengths long. The magnitude of the calculated electric field is shown in Fig. 3 as a colour map with azimuthal and polar angles as axes. Fig. 3(a) concerns the radial component, while Figs. 3(b) and 3(c) represent polar and azimuthal components, respectively. We can observe that behind the FGP the strength of the field is not negligible. Figs. 4(a), (b) and (c) show the field components obtained using the proposed method, the polar axis is limited to the interval $\lfloor 0°, 90° \rfloor$ since for angles larger than 90° the field is vanishing. The accuracy of this method can be observed by means of the relative error shown in Figs. 5(a), (b) and (c) which is less than one per cent for all field components.

5. CONCLUSION

The proposed method works for flat and thin ground planes independently of their size or their shape, i.e., both circular and polygonal ground planes can be used. The method is not dependent on the kind or on position of the antenna, and can be used for flush-mounted antennas, monopoles and dipoles placed at the centre as well as sideways in respect to the finite ground plane. It can obviously be applied to the measured field of antennas in free-space in order to obtain their characteristics when placed in front of an infinite ground plane. A particular advantage of this technique is its easy implementation in existent measurement systems such as near-field multi-probe systems which, generally, handle the measured field by means of a spherical wave expansion.

ACKNOWLEDGMENT

The author wish to thank SATIMO SA for financial support and G. Marrocco and P. Tognolatti for their keen interest and helpful comments.

REFERENCES

1. Cui, B., J. Zhang, and X.-W. Sun, "Single layer microstrip antenna arrays applied in millimiter-wave radar front-end," *Journal Electromagnetic Waves and Applications*, Vol. 22, No. 1, 3–15, 2008.

2. Cui, B., C. Wang, and X.-W. Sun, "Microstrip array double-antenna (MADA) technology applied in millimeter wave compact radar front-end," *Progress In Electromagnetics Research*, PIER 66, 125–136, 2006.
3. Yuan, N., X.-C. Nie, Y.-B. Gan, and T. S. Yeo, "Accurate analysis of conformal antenna arrays with finite and curved frequency selective surfaces," *Journal Electromagnetic Waves and Applications*, Vol. 21, No. 13, 1745–1760, 2007.
4. Hussein, K. A., "Efficient near-field computation for radiation and scattering from conducting surfaces of arbitrary shape," *Progress In Electromagnetics Research*, PIER 69, 267–285, 2007.
5. Ouyang, J., F. Yang, S. W. Yang, and Z. P. Nie, "Exact simulation method VSWIE+MLFMA for analysis radiation pattern of probe-feed conformal microstrip antennas and the application of synthesis radiation pattern of conformal array mounted on finite-length PEC circular cylinder with DES," *Journal Electromagnetic Waves and Applications*, Vol. 21, No. 14, 1995–2008, 2007.
6. Akdagli, A., "An empirical expression for the edge extension in calculating resonant frequency of rectangular microstrip antennas with thin and thick substrates," *Journal Electromagnetic Waves and Applications*, Vol. 21, No. 9, 1247–1255, 2007.
7. Gustafsson, M., "Surface integrated dipole arrays with tapered resistive edge sheets," *Journal Electromagnetic Waves and Applications*, Vol. 21, No. 6, 713–718, 2007.
8. Gustafsson, M., "RCS reduction of integrated antenna arrays with resistive sheets," *J. Electro. Waves Appl.*, Vol. 20, No. 1, 27–40, 2006.
9. Yang, F., V. Demir, D. A. Elsherbeni, A. Z. Elsherbeni, and A. A. Eldek, "Enhancement of printed dipole antennas characteristics using semi-EBG ground plane," *Journal Electromagnetic Waves and Applications*, Vol. 20, No. 8, 993–1006, 2006.
10. Ali, M. and S. Sanyal, "A numerical investigation of finite ground planes and reflector effects on monopole antenna factor," *Journal Electromagnetic Waves and Applications*, Vol. 21, No. 10, 1379–1392, 2007.
11. Bhattacharyya, A. K., "Effects of finite ground plane on the radiation characteristics of a circular patch antenna," *IEEE Trans. Antennas Propagat.*, Vol. 38. No. 2, 152–159, February 1990.
12. Namiki, T., Y. Murayama, and K. Ito, "Improving radiation-pattern distortion of a patch antenna having a finite ground plane," *IEEE Trans. Antennas Propagat.*, Vol. 51, No. 3, 478–482, March 2003.

13. Williams, J. T., H. J. Delgado, and S. A. Long, "An antenna pattern measurement technique for eliminating the fields scattered from the edges of a finite ground plane," *IEEE Trans. Antennas Propagat.*, Vol. 38, No. 11, 1815–1822, November 1990.
14. Griffin, D. W., "Monopole Antenna method of diagnosing the effectiveness of ground plane edge scattering elimination technique," *IEEE Antennas Propagat. Int. Symp. Dig.*, 223–226, May 1982.
15. Wang, R. W. and V. V. Liepa, "Reduction of the edge diffraction of a circular ground plane by using resistive edge loading," *IEEE Antennas Propagat. Int. Symp. Dig.*, 769–771, June 1985.
16. Burrell, G. A. and A. R. Jiamieson, "Anennas radiation pattern measurement using time-to-frequency transformation (TFT) techniques," *IEEE Trans. Antennas Propagat.*, Vol. 21, 702–704, September 1973.
17. Clouston, E. N. and S. Evans, "Time-domain techiniques for the measurement of narrow-bandwidth antenna parameters," *IEEE Antennas Propagat. Int. Symp. Dig.*, 308–311, June 1988.
18. Kouyoumjian, R. G. and P. H. Pathak, "A uniform geometrical theory of diffraction for an edge in a perfectly conducting surface," *Proc. IEEE*, Vol. 62, No. 11, 1448–1461, November 1974.
19. Yaghjian, A. D., "An overview of near-field antenna measurements," *IEEE Trans. Antennas Propagat.*, Vol. AP-34, 30–45, Jan. 1986.
20. Costanzo, S. and G. Dimassa, "Direct far-field computation from bi-polar near-field samples," *Journal of Electromagnetic Waves and Applications*, Vol. 20, No. 9, 1137–1148, 2006.
21. Costanzo, S. and G. di Massa, "Far-field reconstruction from phaseless near-field data on a cylindrical helix," *Journal of Electromagnetic Waves and Applications*, Vol. 18, No. 8, 1057–1071, 2004.
22. Ayestar, R. G. and F. Las-Heras, "Near field to far field transformation using neural networks and source reconstruction," *Journal of Electromagnetic Waves and Applications*, Vol. 20, No. 15, 2201–2213, 2006.
23. Koivisto, P. K. and J. C.-E. Sten, "On the in fluence of incomplete radiation pattern data on the accuracy of spherical wave expansion," *Progress In Electromagnetics Research*, PIER 52, 185–204, 2005.
24. Persson, K. and M. Gustafson, "Reconstruction of equivalent currents using a near-field data transformation with radome

applications," *Progress In Electromagnetics Research*, PIER 54, 179–198, 2005.

25. Ferrara, F., C. Gennarelli, R. Guerriero, G. Riccio, and C. Savarese, "An efficient near-field to far-field transformation using the planar wide-mesh scanning," *Journal of Electromagnetic Waves and Applications*, Vol. 21, No. 3, 341–357, 2007.
26. Iversen, P. O., Ph. Garreau, and D. Burrell, "Real-time spherical near-field handset antenna measurements," *IEEE Antennas and Propagations Magazine*, Vol. 43, No. 3, 90–95, June 2001.
27. Bolomey, J. C., B. J. Cown, G. Fine, L. Jofre, M. Mostafavi, D. Picard, J. P. Estrada, P. G. Friederich, and F. L. Cain, "Rapid near-field antenna testing via arrays of modulated scattering probes," *IEEE Trans. Antennas Propagat.*, Vol. 36, No. 6, 804–814, June 1988.
28. Laitinen, T. A., J. Ollikainen, C. Icheln, and P. Vainikainen, "Rapid spherical field measurement system for mobile terminal antennas," *IEEE Instrumentation and Measurement Technology Conference (IMTC'03)*, 968–972, Vail, CO, USA, May 20–22, 2003.
29. Laitinen, T., J. Toivanen, C. Icheln, and P. Vainikainen, "Spherical measurement system for determination of complex radiation patterns of mobile terminals," *Electron. Lett.*, Vol. 40, No. 22, 1392–1394, 2004.
30. Hansen, J. E., *Spherical Near-Field Antenna Measurements*, Peter Peregrinus, London, U.K., 1988.
31. "FEKO User's Manual, Suite 5.1," EMSoftware & Systems-S.A. (Pty) Ltd. [Online]. Available: http://feko.info, Stellenbosch, South Africa, December 2005.